Surface & Coatings Technology 205 (2011) 5103–5108

Contents lists available at ScienceDirect

Surface & Coatings Technology

journal homepage: www.elsevier.com/locate/surfcoat

Effect of a superhydrophobic coating on the combustion of aluminium and iron oxide nanothermites

Eric Nixon [a], Michelle L. Pantoya [a,*], Ganapathy Sivakumar [b], Ashwin Vijayasai [b], Tim Dallas [b]

[a] Mechanical Engineering Department, Texas Tech University, Lubbock, TX, 79409, United States
[b] Electrical and Computer Engineering Department, Texas Tech University, Lubbock, TX7, 9409, United States

ARTICLE INFO

Article history:
Received 14 October 2010
Accepted in revised form 15 May 2011
Available online 23 May 2011

Keywords:
Superhydrophobic coating
Thermite
Combustion
Submerged reactions
Nanoenergetic

ABSTRACT

There is an interest in broadening the range of applications of nanoenergetic composite materials to include their combustion and energy generation in submerged environments. Currently, their use is primarily limited to gas environments. Oceanic power generation, underwater ordnance, propulsion, metal cutting, and torch technologies are examples of applications that would significantly benefit from nanocomposite energetic materials. Recent research on superhydrophobic coatings has made it possible to coat nanoenergetic samples using a vapor-phase deposition process which significantly reduces the detrimental effects of water entering the composite that can occur during wet-chemistry based superhydrophobic processes. In this work, we discuss the process utilized to produce the superhydrophobic coating on nanoenergetic materials. We then analyze the bubble energy produced and compare this value to other energetic formulations. It was found that the ratio of the bubble energy to the total energy of combustion was an order of magnitude higher for the superhydrophobic coated materials compared to energetic composites containing a hydrophobic binder.

1. Introduction

Reducing the functional structure size to the nanoscale has allowed many critical advances in the development of technologically important materials, including energetic materials. Particle reactants now synthesized on the nanometric-scale have resulted in unique combustion behaviors. Nanocomposite energetic materials (NEMs) can include thermites and reactive materials, and are described here as a metal fuel combined with a metallic oxide, or other organic or inorganic binder. NEMs containing nanometric aluminum (nm-Al) have been studied extensively [1–3]. Ignition sensitivity [4] and flame propagation rate [5] are two parameters that show orders of magnitude enhancements when reactants are composed of nm-Al particles. Ignition sensitivity describes the energy threshold over which a reaction will self propagate to completion. Enhanced ignition sensitivity associated with nanoparticles is associated with reduced ignition energy thresholds over their micron scale counterparts. Flame propagation rate is the speed a reaction wave will propagate through the reactant mixture. Enhanced flame propagation rates are associated with increased speeds.

Compared to monomolecular energetic materials (i.e., explosives such as TNT), NEMs hold great promise owing to their high heats of combustion (Table 1). The heat of combustion data shown in Table 1 was generated using a thermal equilibrium software program, REAL (Tim Tech, LLC) for the stoichiometric reactions. While NEMs provide high energy densities, their reactive power is limited by the reaction mechanism. Monomolecular reactions are kinetically controlled by a rapid sequence of bond breaking within the molecular structure [6]. In contrast, NEMs reactions are controlled by the mass and energy diffusion between reactants and limited by the diffusion distance between fuel and oxidizer particles [6]. This diffusion mechanism limits the reactive power of NEMs. Monomolecular formulations may exhibit lower heats of combustion (Table 1), but that energy is delivered over shorter durations enabling significantly more reactive power associated with monomolecular materials [6].

There has been much research reported on the underwater blast characterizations of monomolecular materials (such as TNT). Vadhe et al. [7] provide a recent review of much of the literature. The realm of applications for NEMs may grow tremendously in the near future, but will be limited to environmental constraints surrounding the reaction. For example, NEMs cannot react underwater without a hydrophobic binder. This is primarily due to the fact that water permeates the consolidated reactant mixture resulting in (1) breaking apart the reactants prior to ignition and reaction; or (2) immediate quenching of the reaction upon ignition. It is noted that if water is combined with nanometric aluminum in stoichiometric proportions, nanometric aluminum is capable of reacting with water as the sole oxidizer [8]. There are a myriad of applications that would benefit from NEMs that are combustible in aqueous environments. These applications include: fuses, propulsion, underwater ordnance, torch and metal cutting technologies, off shore oil drilling, blasting and welding, as well as alternative power sources in oceanic environments.

* Corresponding author. Tel.: +1 806 742 3563; fax: +1 806 742 3540.
E-mail address: michelle.pantoya@ttu.edu (M.L. Pantoya).

0257-8972/$ – see front matter © 2011 Elsevier B.V. All rights reserved.
doi:10.1016/j.surfcoat.2011.05.014

Table 1
Heat of combustion for various monomolecular and NEMs.

Reactant composition	Heat of combustion (kJ/kg)
$C_7H_5N_3O_6$ (TNT)	1362
$2Al + Fe_2O_3$	3743
$4Al + 3\text{-}C_2F_4$–(Teflon™)	10,709

Some attempts have been made to include a hydrophobic binder in the formulation to prevent water permeation. This led to a breakthrough in the understanding of how only nanometric aluminum particles with increased ignition sensitivity lead to reaction underwater [9]. On the micron-scale, aluminum lost more heat to the water surroundings than required for reaction propagation such that the reaction quenches [9]. Nanometric aluminum powder has been incorporated into explosive formulations for underwater applications [10]. Also, prior to the advent of nanotechnology, some thermite formulations had been used as underwater flares [11].

The pit-fall of the hydrophobic binder assembly, which was a reactive material consisting of nanometric aluminum combined with polytetrafluoroethalyene (Teflon), was that water may have participated in the reaction such that the overall energy available from the Al-Teflon reaction could not be fully attained. An alternative is to coat a consolidated thermite with a superhydrophobic coating that would enable reaction underwater while also limiting the participation of the environment in the reaction.

The goal of this work was to produce a NEMs that can react underwater. The objectives were to coat a NEM formulation of aluminum combined with iron oxide (Al–Fe_2O_3) with a superhydrophobic coating and quantify the bubble energy in an effort to characterize the reaction dynamics associated with submerged, NEMs formulations.

2. Experimental

2.1. Materials

Slightly fuel rich (equivalence ratio 1.1) mixtures of Al–Fe_2O_3 were prepared using 80 nm average diameter Al (Novacentrix) or 1–3 μm average diameter Al (Atlantic Equipment Engineers) combined with nanometric Fe_2O_3, (50 nm diameter, Novacentrix). Mixtures were prepared by combining the powders in controlled proportions in hexanes. The powder solution was mixed using an ultrasonification process described in detail in Granier et al. [4], but summarized briefly here. The sonification process helps break up large agglomerates and ensure a more homogenous mixture. The mixture was heated at low temperature in a glass dish to evaporate the solution. The composite powder was collected and pressed into pellets at approximately 50% of the theoretical maximum density (TMD) resulting in approximately 250 mg samples. The pressing process is described in detail elsewhere [12].

2.2. Coating deposition

The degree of hydrophobicity of a surface is typically quantified using a goniometer which measures the contact angle between a water (or other fluid) droplet and a surface [13]. Static contact angles below 90° are considered hydrophilic and values above 90° are considered hydrophobic. A standard fluorocarbon coating on a smooth surface will produce a contact angle of ~110°. Contact angles above ~150° are considered super-hydrophobic [14]. The super-hydrophobic surface property is made possible by combining nano-texturing of the surface with a low surface energy coating on top of it.

In order to compare the effect of the coatings, three types of pellets were produced: one set had a fluorocarbon coating, one set had an alumina nanoparticle and fluorocarbon coating, and one set was uncoated. We used a commercially available deposition system (RPX 550 from Integrated Surface Technologies, Inc.) to produce the various coatings. In order for a surface to have superhydrophobic properties, there needs to be micro/nanoscale surface roughness and the surface has to have a very low surface-energy. The surface roughness can already be present, or added by the coating system.

The system utilizes a sequential vacuum deposition process to apply nanoparticles through a hybrid ALD (Atomic Layer Deposition) — CVD (Chemical Vapor Deposition) process. This step is followed by a CVD deposited adhesion promotion coating (silsesquioxane layer [15]). The nanoparticle decorated surface can then be capped by a low surface energy fluorocarbon SAM (self-assembled monolayer). As illustrated in Fig. 1, the superhydrophobic nanocoating consists of alumina nano-particles, the adhesion layer, and the fluorocarbon monolayer. All steps are carried out in a pressure range of 0.02–10.4 Torr. The deposition chamber will allow substrate sizes up to ~900 cm^2 to be coated, although the pellets were on the order of 1.5 cm^2.

2.3. Coating system

The coating system is shown in Fig. 2. The chamber includes inlets for a maximum of five precursor chemicals. The chamber is also connected to a mechanical pump for evacuating the chamber. An applicator plate that is permeated with numerous holes is used to disperse the chemistries over the substrate. The substrate(s) to be coated is placed beneath the applicator plate. Pneumatic valves are digitally actuated with high precision using LabVIEW control software. For the coatings described in this article, the temperature of the chamber was maintained at 45 °C. The temperatures of the chamber and the various inlet precursors can be changed as per user needs. The precursors are stored in cartridges (cartridges have temperature control — to modify vapor pressure of precursors). The precursors exit from the cartridges and flow through its corresponding stick; the stick temperature of each precursor is maintained at 5 °C more than its corresponding cartridge temperature (this is to prevent condensation of the chemical as it flows from the cartridge to the stick). The functionalization precursor tridecafluoro-1,1,2,2-tetrahydrooctyltrichlorosilane (FOTS) is maintained at 95 °C (while its stick temperature is maintained at 100 °C). A curve trace shows the pressure variation as the deposition process is carried out. The pressure inside the chamber is controlled by a mechanical pump. After deposition or in the intermediate steps of the deposition process, the residual vapors are pumped/purged out of the chamber with nitrogen gas.

2.4. Reaction chemistry

The reaction that describes the formation of alumina nanoparticles is given below [15, 16]:

$$2Al(CH_3)_3 + 3H_2O \rightarrow Al_2O_3 + 6CH_4. \quad (1)$$

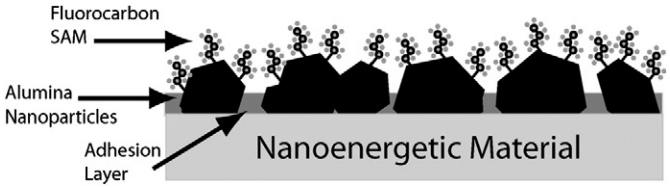

Fig. 1. Conceptual picture of nanoenergetic material coated with alumina nanoparticles, an adhesion promoting layer, and a fluorocarbon SAM top coating.

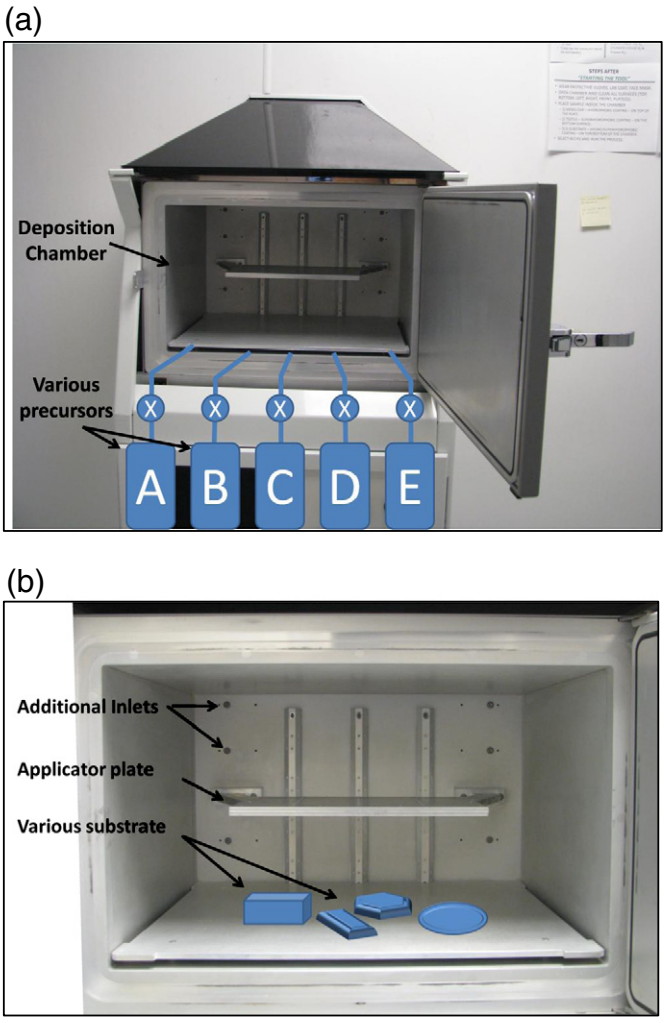

Fig. 2. Schematic diagram of the coating system. (a) This shows the various precursors entering the system, sequential/concurrent inlet of the precursors is possible. (b) This shows the chamber. Substrates are placed beneath the applicator plate for super-hydrophobic coating.

This reaction can also be limited to two-step self-limiting reactions [15, 16]. The reaction takes place in a low pressure (20 mTorr) reaction chamber, As mentioned in Eq. (1), the Tri-methyl Aluminium (TMA) is injected in the chamber (0.16 Torr), followed sequentially by a water-alcohol mixture (0.55 Torr). The injection of both these reactants causes the formation of alumina nano-particles in the chamber. These nano-particles range in size from 50–200 nm

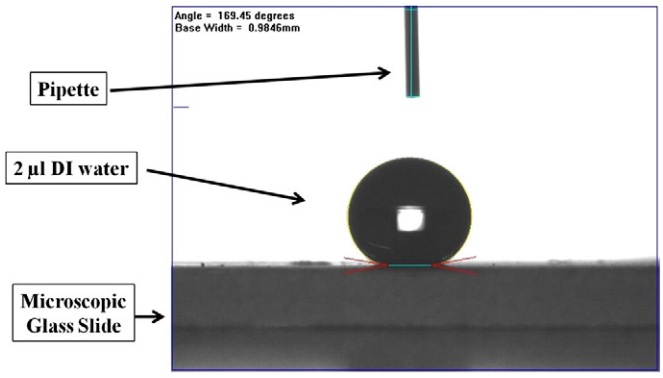

Fig. 3. Contact angle result of DI water on witness sample.

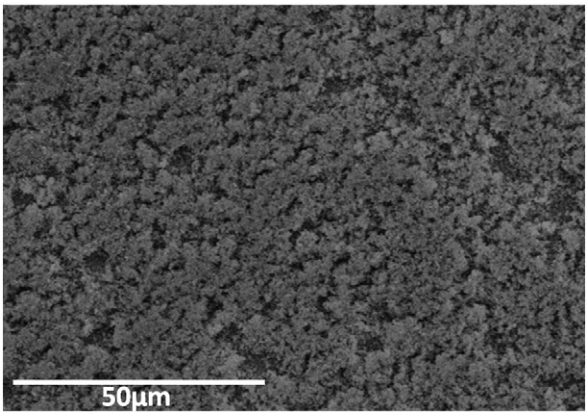

Fig. 4. SEM image of highly conformal coating on the witness sample.

[17] and deposit on to the NEMs pellets. A linking chemistry is subsequently injected into the chamber. This process encourages the linking of the nano-particles with each other and also the substrate (also called as adhesion promotion). The reaction chemistry is shown below.

$$SiCl_4 + 2H_2O \rightarrow SiO_2 + 4HCl \quad (2)$$

$$C_2H_4Cl_6Si_2 + 6H_2O \rightarrow SiO_x - (CH_2)_2 - SiO_x + 6HCl + 3H_2O \quad (3)$$

$$C_6H_{12}Cl_6Si_2 + 6H_2O \rightarrow SiO_x - (CH_2)_2 - SiO_x + 6HCl + 3H_2O. \quad (4)$$

$SiCl_4$ is injected into the chamber (0.40 Torr) and it is followed by water–alcohol mixture (3.52 Torr). The adhesion promotion is the linking chemistry shown in Eqs. (2), (3) and (4). The alkyl bridge silanes are the adhesion promoters for the nano-particles and the substrate. The nano-particle deposition and linking processes are repeated three times to produce a nearly conformal coating. The time duration for the entire three step process is 10 min. The temperature of the injection vapor is maintained at 40 °C.

The final step is the deposition of low surface-energy monolayer. This process involves the injection of water–alcohol mixture and the FOTS. The injection is performed at 0.25 Torr. The temperature of the injection vapor is maintained at 95 °C. The high temperature ensures better bonding of the FOTS to the nano-particles. The reaction time for this step is 5 min.

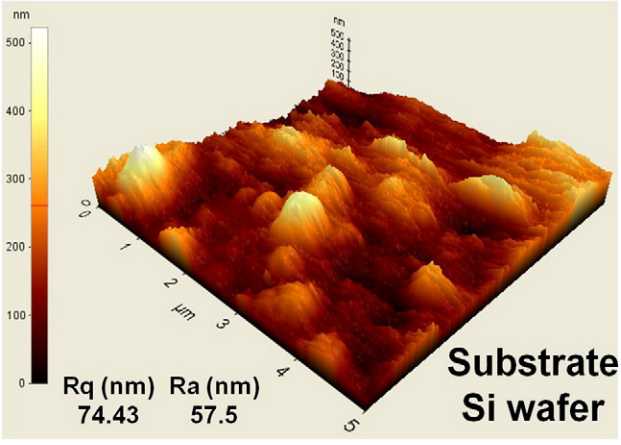

Fig. 5. AFM 3D image of nano-particles on witness sample.

The vapor phase pre-cursors reduce the volume of chemicals needed. Very little of the chemical precursors is wasted, virtually eliminating disposal costs associated with analogous wet-process chemistries. The technique is ideal for coating NEMs because it allows them to be coated by vapor phase technology. The NEMs are pressed together which could allow water to enter the material during wet chemistry superhydrophobic processing. There is no such issue with the vapor phase deposition process. The process can be carried out in ~1 h allowing many samples to be coated on a daily basis.

3. Results and discussion

3.1. Coating characterization

During the deposition, plasma cleaned microscopic glass slides were placed in the chamber and used as witness samples. These sample are used for characterizing the coating. Characterizations of the coatings included contact angle measurements, scanning electron microscopy (SEM), transmission electron microscopy (TEM), fourier-transform infrared spectroscopy (FTIR). For the contact angle measurements, a de-ionized water droplet (2 μl) is pipetted on to the surface of the witness sample. A goniometer (Rame-Hart model 200) was employed to capture the contact angle of the drop on the sample surface. Image J software was implemented to find the contact angle. Multiple locations on the surface of the witness samples were measuremed. After multiple trials the average contact angle was found to be ~169°, indicating exceptional superhydrophobicity. Fig. 3 shows one of the images obtained during contact angle measurement.

Fig. 4 shows an SEM image (Hitachi S3400N) of the superhydrophobic coating on a witness sample. The sample preparation for the SEM imaging included deposition of a 2 μm gold coating. The gold layer increases conduction of the specimen and aids in emitting secondary electrons. Fig. 5 shows a very rough surface with occasional voids.

Transmission electron microscope imaging revealed approximately spherical shaped nano-particles with size ranging from ~10–60 nm. Atomic force measurements were also taken to measure the rms height of the nano-particles (~75 nm). Fig. 5 shows an AFM image (Park Systems #XE-100, with K-tek nano # VIT-P probe) measured on a silicon wafer witness sample. The SEM image is used to observe the conformality of the coating, whereas the combination of TEM and AFM results are used to quantify the nano-particle size.

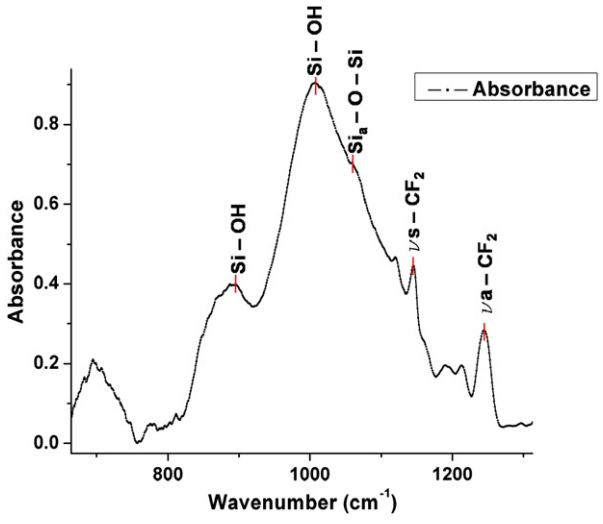

Fig. 6. Magnified section of the FTIR spectra highlighting the peaks and associated modes.

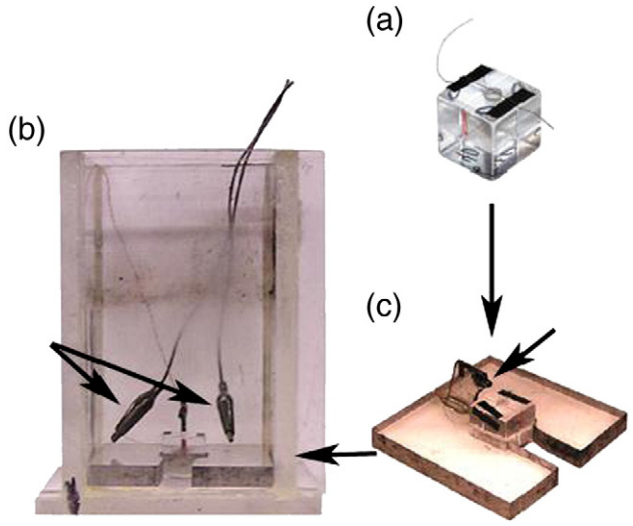

Fig. 7. (a)Tank setup including the sample block, (b) Ignition wire leads, and (c) Underwater blast pressure sensor.

Infrared spectra of the deposited superhydrophobic coating were taken using a Perkin-Elmer Spectrum One system. Witness samples were used for the FTIR analysis. Fig. 6 shows the important region of the spectrum from the superhydrophobic coating. Analyzing the spectra allows molecular vibrations and stretching vibrations of various bonds in the coating can be identified. One of the peaks identified is the Si-O-Si stretching mode at 1059 cm^{-1}[18–21]. The CF_2 stretching mode is divided into two peaks, 1245 cm^{-1} corresponds to the CF_2 asymmetric stretching ν_a; the CF_2 symmetric stretching mode, ν_s, is at 1145 cm^{-1} [22]. The trisilanol portion of the SAM is identified in two locations, 1007 cm^{-1} and 896 cm^{-1} [20]. Other peaks in the plot are attributed to O–H modes. Chryssou et al. have used a CVD process for deposition of Al_2O_3 nano-particles [23]. Their results on FTIR spectra for Al_2O_3 mention major absorption bands from 400–1250 cm^{-1}. To identify the peaks of Al–O and Al–O–Al bonds they annealed the alumina to high temperature ~600 °C. We do not have the instruments to perform this experiment to identify the peaks for alumina. However, the SEM/TEM images clearly show the alumina nanoparticles.

3.2. Submerged reaction experiments

Both coated and uncoated pellets were placed in a vertical, cylindrical cavity at the bottom of an acrylic tank and ignited with a

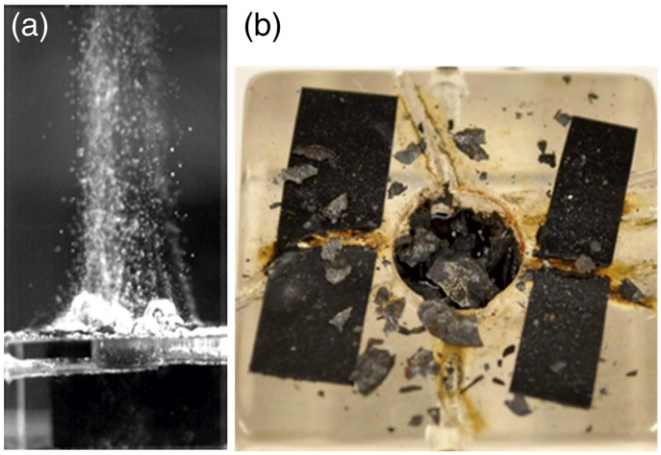

Fig. 8. (a)Out-gasing of a submerged pellet, (b) Resulting pellet fragments.

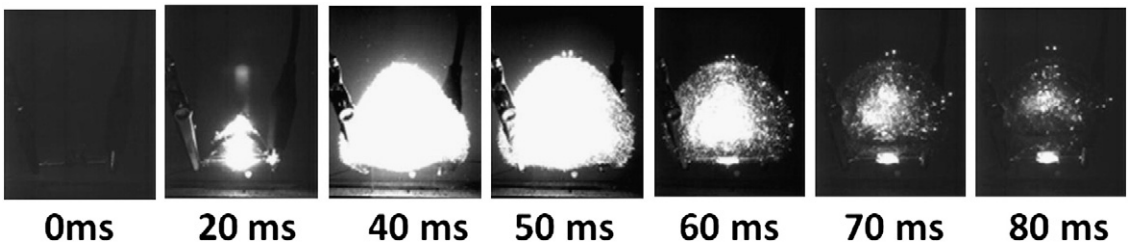

Fig. 9. Still frame images of the super-hydrophobic coated $Al + Fe_2O_3$ reaction submerged underwater at various times.

hot wire. The Al–Fe_2O_3 pellets were ignited while submerged in the aquarium chamber using a hot wire ignition source. More details on the experimental aquarium chamber can be found in [9]. A high speed camera (Phantom v7) capturing images at 10,000 frames per second was used to monitor the reaction hydrodynamics. A fiber optic light guide provided additional illumination to improve visualization. The unique aquarium setup allowed the gas products/water interface to be recorded to estimate the gas generation of a reaction as seen in Fig. 7.

Uncoated pellets experience significant outgassing in a depth of only 3 in. of water. Fig. 8a shows the initial outgassing and Fig. 8b shows the remains of the original pellet after being submerged for 5 days. The superhydrophobic coating prevented outgassing, which allowed the pellet to remain submerged without apparent damage for extended durations (e.g., estimates to date are over 9 months). Fig. 9 shows still-frame images over time (0–80 ms) of the superhydrophobic coated $Al + Fe_2O_3$ reaction submerged underwater.

An analysis of the volume of the bubble enables the amount of energy used for the water displacement to be computed and this displacement energy (E_d) is referred to here as bubble energy (Eq. (5)).

$$E_d = \frac{V_{bubble} \cdot P_{hydrostatic}}{M_{sample}}. \quad (5)$$

Since the height of the bubble is small, the differences between the hydrostatic pressure at the top and bottom of the bubble are approximated to be equal. The bubble can be seen to have vertical symmetry, but no horizontal symmetry is present. To calculate the volume (V), the bubble shape is approximated to be an ellipsoid. The mass of the sample (M) allows the energy to be normalized, and therefore the results will be comparable to similar tests.

Table 2 shows results for displacement energy for each experiment and coating type. Both the pellets coated with the alumina and fluorocarbon, as well as the pellets coated only with the fluorocarbon produced results within the experimental uncertainty of the measurements such that no significant deviation in reactive behavior was observed. The largest contribution to uncertainty is in the repeatability of the measurement. For both coatings, five pellets were examined. The average bubble energy of the coated (hydrophobic and superhydrophobic) $Al + Fe_2O_3$ pellets is 171 ± 5 kJ/kg. The nanocoating particles were not observed to permeate the NEMs. Based on the burn rate, it does not appear the fluorocarbon layer has significantly permeated the nano-particles and the adhesive layer. While the combustion behavior of the two different coatings was not observed to be significantly different, the alumina and fluorocarbon coating may improve long term water exclusion.

The coated $Al + Fe_2O_3$ pellets demonstrate a significant improvement over the 92 kJ/kg bubble energy measured from the Al–Teflon submerged reaction [9]. The ratio of the bubble energy to the heat of combustion for these NEMs (Table 1) is 0.04 for Al–Fe_2O_3 and 0.0086 for the Al–Teflon NEMs. Because these reactions are submerged, there is considerable energy loss to the surroundings but the coating allows an order of magnitude increase in energy available and presents new potential for integrating NEMs into submerged reaction applications.

Table 2
Displacement energy results as a function of pellet coating.

Coating	Test	E_d
Fluorocarbon	1	174
Fluorocarbon	2	172
Fluorocarbon	3	171
Fluorocarbon	4	169
Fluorocarbon	5	168
Alumina/fluorocarbon	1	166
Alumina/fluorocarbon	2	169
Alumina/fluorocarbon	3	171
Alumina/fluorocarbon	4	173
Alumina/fluorocarbon	5	176

4. Conclusions

This study showed that nanothermites can be coated with a vapor-phase deposited superhydrophobic coating that prevents water permeation of the reactants and enables NEMs reaction in submerged environments. This is a novel approach to underwater NEM combustion that previously required the integration of a hydrophobic material into the reactant formulation. With this low-pressure, low-temperature CVD/MVD coating technology, the results presented here suggest any formulation can be prepared for submerged reaction. These results imply that coated NEMs formulations may produce significant advances in underwater energetic materials technology.

Acknowledgements

Authors E. Nixon and M. Pantoya acknowledge continued support and helpful discussion with Dr. Ralph Anthenien, ARO contract number W911NF0410217. Authors T. Dallas, G. Sivakumar, and A. Vijayasai acknowledge the support from the National Science Foundation (CBET #0821162); SEM/TEM imaging provided by Charles Linch, Texas Tech University Health Sciences Center Imaging Center; AFM imaging facility provided by Dr. Brandon Weeks, Texas Tech University, Chemical Engineering.

References

[1] E.L. Dreizin, Pror. Energy Combust. Sci. 35 (2009) 141.
[2] R.A. Yetter, G.A. Risha, S.F. Son, Proceedings of the Combustion Institute 32 (2) (2009) 1819.
[3] M.L. Pantoya, J.J. Granier, Propellants Explos. Pyrotech 30 (1) (2005) 53.
[4] J.J. Granier, M.L. Pantoya, Combust. Flame 138 (4) (2004) 373.
[5] B.S. Bockmon, M.L. Pantoya, S.F. Son, B.W. Asay, J.T. Mang, J. Appl. Physi 98 (6) (2005) 064903.
[6] I. Glassman, R. Yetter, Combustion, 4th edition Elsevier Inc, San Diego, CA, 2008.
[7] P.P. Vadhe, R.B. Pawar, R.K. Sinha, S.N. Asthana, A.S. Rao, Combust. Explos. Shock Waves 44 (4) (2008) 461.
[8] G.A. Risha, S.F. Son, R.A. Yetter, V. Yang, B.C. Tappan, Proceedings of the Combustion Institute 31 (2007) 2029.
[9] S.C. Stacy, M.L. Pantoya, D.J. Prentice, M.A. Daniels, E.D. Steffler, Adv. Mater. Process. 167 (10) (Aug 2009) 33.

[10] E.W., Rolle, Thermite Reaction Underwater Flare, US Patent 3107614 USA (19630029.
[11] L.R. Bates, Mat. Res. Soc. Proc. V. 800 (2004) 257.
[12] M.L. Pantoya, V.I. Levitas, J.J. Granier, J.B. Henderson, J. Propuls. Power 25 (2) (March-April 2009).
[13] T. Ishizaki, N. Saito, Yasushi Inoue, M. Bekke, O. Takai, J. Phys. D. Appl. Phys 40 (2007) 192.
[14] B. Bhushan, Y.C. Jung, Ultramicroscopy 107 (2007) 1033.
[15] J. Chinn, F. Helmrich, R. Guenther, M. Wiltse, K. Hurst, R.W. Ashurst, NSTI nanotech. 1 (2010) 612.
[16] S. M. George and C. F. Herrmann, "AL2O3 atomic layer deposition to enhance the deposition of hydrophobic or hydrophilic coatings on microelectromechanical devices," U.S. patent 0012975, January 20, 2005.
[17] J. M. Chinn, R. Ashurst, A. Anderson, "Surface coating process," U.S. patent 00110819, April 30, 2009.
[18] C.P. Tripp, M.L. Hair, Langmuir 7 (1991) 923.
[19] C.P. Tripp, M.L. Hair, Langmuir 8 (1992) 1120.
[20] C.P. Tripp, M.L. Hair, J. Phys. Chem. 97 (1993) 5693.
[21] J.K. Chen, F.H. Ko, K.F. Hsieh, C.T. Chou, F.C. Chang, J. Vac. Sci. Technol. 22 (6) (2004) 3233.
[22] D. Devaprakasam, S. Sampath, S.K. Biswas, Langmuir 20 (2004) 1329.
[23] C.E. Chryssou, C.W. Pitt, Appl. Phys. 65 (1997) 469.